Journal of Materials Chemistry C

Accepted Manuscript

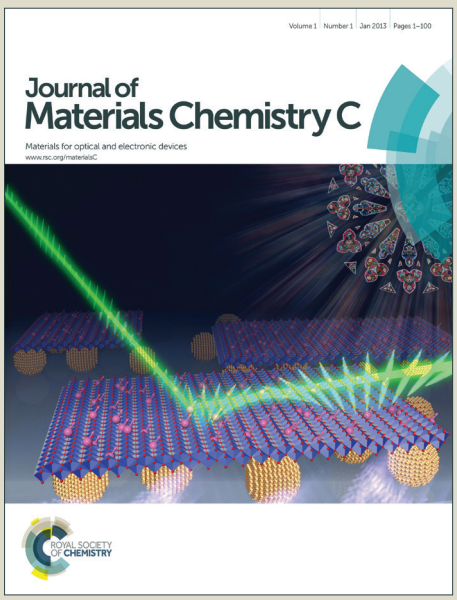

ROYAL SOCIETY OF CHEMISTRY

www.rsc.org/materialsC

Tailored defect induced sharp excitonic emission from microcrystalline CuI and its *ab-initio* validation

Swati Das[1‡], Subhajit Saha[2‡], Dipayan Sen[1‡], Uttam Kumar Ghorai[2] and Kalyan Kumar Chattopadhyay[1,2*]

[1]Department of Physics, Jadavpur University, Kolkata-700032, India

[2]School of Materials Science and Nanotechnology, Jadavpur University, Kolkata-700032, India

ABSTRACT:

Defect rich structures of metal halide based ionic semiconductors are the main problem owing to their prospective applications in a broad range of light emitting devices, such as from ordinary light emitting diodes to more exotic laser diodes. As a consequence of inherently low formation energies of the native defects, especially in cuprous iodide (CuI), it is very difficult to achieve band edge excitonic emission as it is often quenched by defect center mediated radiative recombination. Here in we report an in-situ room temperature technique for fabricating highly crystalline CuI films on transparent and flexible polyethylene terephthalate (PET) substrates. The as prepared samples were found to exhibit signatures of sharp excitonic emission. Optimization of reaction parameters revealed pH of the solution to be a pivotal parameter for controlling such excitonic emissions. Even though all as grown films were observed to be highly crystalline in nature, varying concentration of iodine was found to manifest its effect by evolving crystal morphology from micro rods to polyhedrons. Further theoretical investigations using density functional theory was also carried out to investigate how breakage of Cu-I bond contributes in evolution of such defect states. The less defective films with sharp excitonic band are speculated to be a potential candidate for solid state light emitting devices.

Keywords: CuI; Thin films; Excitonic emission; Photoluminescence; Iodine vacancy

1. INTRODUCTION:

Wide band gap inorganic semiconductors has found themselves at the centerfold of cutting edge research in the last few years due to their promising potential applications towards solid state light emitting devices [1-7]. Commercial availability of GaN based ultraviolet devices has also stimulated the search for other inorganic semiconductors having excellent optoelectronic features. This hunt explored some new class of materials along with the rediscovery of some existing class of compounds. Metal halides like CuX (X=Cl, Br, I) were already known for their high degree of ionic conductivity with Cu^+ ions as the mobile charge carriers [8-10]. Apart from this, metal halides, especially cuprous iodide (CuI) has a unique combination of high excitonic binding energy [11] with excellent transparency [12] throughout the entire visible region which readily proves its capability to be used for transparent excitonic devices.

Since excitonic emission is the most capable luminescence mechanism in solid, it is widely speculated that this phenomenon could be exploited for obtaining highly efficient solid state optoelectronic devices that can be used in numerous practical scenarios. But unfortunately, in case of most of the inorganic covalent semiconductors, as their excitonic binding energies are quiet small, thermal dissociation of excitons leads to very feeble excitonic emission at room temperature. A minimum of 26 meV exciton binding energy is needed to achieve strong excitonic emission at room temperature, and consequently, even for conventional semiconductor light emitting devices like GaN, light emission mechanism is of nonexcitonic nature. This is the point where CuI claims its superiority over other binary semiconductors. It is blessed with high exciton binding energy (62 meV) including large direct band gap (3.1 eV). It is well known that light extraction mechanism in organic light emitting diodes also strongly depends on the excitonic luminescence [13]; but even though having high exciton binding energy, they suffer

some serious drawbacks like poor thermal stability [14] and low electron/hole mobility [15], which reduces the lifetime as well as performance of the devices. However, thermal stability of CuI is much higher, in comparison with the conventional organic semiconductors. Hence, realization of excitonic devices is much easier by using CuI as an active material.

Being inspired by these excellent features, several researchers had devoted their efforts to develop high quality CuI films for practical applications. But, due to defect rich nature CuI, most of them failed to obtain defect free excitonic emission at room temperature. Being an ionic semiconductor, CuI is very prone to contain fundamental native defects like cation and/or anion vacancy and antisite occupation. Upon higher energy excitation, radiative recombination through these defect centers dominates and excitonic emission remains almost forbidden. Hence it imposes a real challenge to develop CuI films which could generate defect free pure excitonic emission. Since the synthesis technique strongly affects the nature of the produced films, it is extremely important to probe the exact synthetic condition for which defect band could arise in the emission spectra. Proceeding in this approach, in recent years, several common thin film deposition techniques ranging from bulky physical deposition (vacuum evaporation [16] magnetron sputtering [17] pulsed laser deposition (PLD) [18]) to chemical routes (successive ionic layer adsorption and reaction (SILAR) [19], sonochemical [20], electrochemical [21]) have been adopted for preparation of CuI films. In these reports however, not only the production of films were associated with complex synthesis protocol or costly deposition equipments, but also the origin of the defect band in the emission spectra remained unclear. Moreover, such films grown on the rigid substrates like glass and silicon fail to fulfill the requirements for cutting edge flexible electronic devices. Hence, a focused study directed towards the basic understanding of

the exact experimental condition which originates the defect band in the emission spectra is highly necessary.

In the present work, we report a simple inexpensive technique for fabrication of highly crystalline CuI films on transparent and flexible poly ethylene terephthalate (PET) substrate. Strength of the acidic environment played a crucial role to develop CuI films with different type of surface morphology. The detail investigation of the optical property shows higher concentration of iodine leads to almost defect-free excitonic emission at room temperature. Appearance of the defect band in the emission spectra is also probed theoretically with the help of density functional theory (DFT) and it was found that deficiency of iodine in the CuI lattice generated the surface trap states near the valence band maxima, at which the trapped holes recombine with the relaxed electrons to produce defect band in the photoluminescence (PL) spectra. The obtained results clearly indicate that the synthesized films have great potential for application in solid state lighting like near UV LEDs and laser diodes.

2. EXPERIMENTAL SECTION:

Preparation of CuI thin film by chemical bath deposition: In the typical synthesis process, at first, using tungsten boat, thin film of copper was deposited on PET substrate by thermal evaporation technique in a high vacuum chamber ($2x10^{-6}$ Pa) at a constant current (60 mA). After that, two solutions were made separately by adding an adequate amount of hydroiodic acid (HI) in 30 ml deionized water to maintain the pH 1 and 3. Then the copper deposited PET substrates were immersed in these acidic solutions and kept in culture bottle for several hours at room temperature. A full replacement of the pre deposited Cu layer took place by formation of pale yellow coloured CuI film on the PET substrate after several hours. The films were then

washed several times by deionized water and ethanol to remove the residual reactants and were kept at vacuum oven for overnight for drying. The digital images of the Cu deposited PET films before and after HI addition is shown in Figure S1 of Electronic Supplementary Information (ESI).

3. RESULTS & DISCUSSION:

3.1. Structural and compositional analysis:

The typical X-ray diffraction (XRD) pattern of the CuI films is shown in figure 1, in which all diffraction peaks were assigned to a cubic phase γ-CuI [marshite: JCPDS 06-0246, F3m (216)] with calculated lattice constant a = 6.05 Å. The well assigned diffraction peaks with no other unwanted signals confirmed the phase purity of the deposited films. The sharp characteristics of all the synthesized films clearly indicate that the films were highly crystalline in nature.

Formation of pure phase CuI along with the chemical composition of the elemental components was further justified by energy dispersive X-ray (EDX) and X-ray photoelectron spectroscopy (XPS) analysis. The detailed compositional analysis, done by EDX, is represented in figure 2(a) & (b). Both the films were consisted of two major peaks corresponding to Cu and I whose atomic ratio was found to be dissimilar due to the different concentration of HI in the nutrient solution. The atomic ratio of Cu and I obtained from EDX analysis was 1.13:1 and 1:1.03 for pH3 and pH1, respectively. The opposite nature of Cu and I is clearly noticeable in the atomic ratios obtained from the EDX data. Due to the large difference in the ionic radius of Cu^{+} and I^{-}, tightly packed CuI crystal always has a high probability of iodine vacancy formation within the cell [22]. Apart from that, lower concentration of HI at pH3 instinctively generates iodine vacancy within the corresponding CuI films, which is reflected from the EDX data. But, the higher

concentration of HI at pH1 compensates this deficiency of iodine and makes the corresponding CuI films slightly iodine rich.

Further investigation of the exact chemical states of the constituent elements within the synthesized thin films was carried out by detailed XPS analysis. All the spectra have been charge corrected by taking the peak of C 1s at 284.6 eV which appeared due to the presence of adventitious carbon on the surface of the samples during atmospheric exposure. The presence of Cu and I with no other impurity signals in the typical survey scan (shown in Figure S2 of ESI) reflects pure phase formation of CuI. The high resolution core level spectra for Cu 2p (shown in fig. 2(c)) consists of two peaks at 952.2 and 932.2 eV, which corresponds to Cu $2p_{1/2}$ and Cu $2p_{3/2}$, respectively. The absence of any shake up satellite peak strongly claims the +1 oxidation state of Cu, which is the basic requirement for CuI formation. The peaks located at 619.5 and 631 eV (shown in fig. 2(d)), are well consistent with I $3d_{5/2}$ and I $3d_{3/2}$ core level spectra of I^- ,respectively, [23]. A careful observation of the high resolution spectra of Cu 2p and I 3d evidently reveals that all the spectra are not exactly in the same binding energy value for both the films, rather a minute shift in their binding energy value can be observed. The higher binding energy shift along with reduced intensity of I 3d peaks for pH3 films can be directly attributed to the presence of iodine vacancy in the corresponding films. This phenomenon is already supported by the earlier reports which indicate that formation of anion vacancy is always associated with the higher binding energy shift of the corresponding core level spectra [24, 25]. But such a small amount of iodine vacancy was not sufficient to reduce the surrounding Cu^+ ions and as a result, the Cu 2p peaks remains almost unaltered. Hence, the presence of only monovalent Cu ions is firmly established from the absence of any unwanted peaks within the Cu 2p spectra.

3.2. Microstructural analysis and the growth mechanism:

FESEM and TEM images of the synthesized films are shown in the figure 3. It is quite clear from the Figure 3(a) that the grown CuI film was composed of truncated tetrahedron to octahedron like crystal shape all over the substrate's surface with a wide size distribution from 500 nm to 2 μm. To get a better insight into the formation of microstructure, we performed HRTEM analysis. Figure 3(b) depicts the typical TEM image of the octahedron shaped CuI formed by eight {111} facets where four {111} facets are edge-on when viewed along [110] direction. The HRTEM image (shown in figure 3(c)) also shows the regular lattice fringes of the octahedrons having an inter-planar spacing of d~ 0.213 nm, corresponding to (220) plane of γ-CuI. Figure 3(e), illustrates the morphological pattern at higher concentration of iodine ions (~pH1). Different concentration of HI in solution controls the diffusion rate of iodine ions, which emphatically is the key factor for the formation of different morphology of the as grown CuI films. From FESEM observation it can be realized that the higher iodine concentration possesses a favorable site for the formation of micro rod-like morphology. On the basis of the observation, it can be seen that most of the rods possess a well-defined cuboid shape with varying lengths (~2 to 6 μm) and widths (~ 500 to 900) nm. However, the surfaces of these rods are smooth but the edges/tips are truncated. A typical TEM image of the micro rods is shown in Figure 3(f). The characteristic HRTEM image in figure 3(g), clearly exhibits highly crystalline lattice fringes with an estimated inter planar spacing of d~ 0.213 nm, corresponding to (220) plane of γ-CuI. The SAED pattern furthermore shows that the elongation of the rod is along one [110] direction. From the SAED pattern, it is also clear that the rod reflects the exact pattern as of in truncated tetrahedron. Certainly, it can be speculated that these rods are nothing but sidewise joined truncated tetrahedrons.

Moreover, the corresponding SAED pattern with well-defined spots reveals that CuI polyhedron as well as the micro-rods are single crystalline in nature (Figure 3(d) and 3(h)). A precise control over the concentration of HI is a necessary parameter in this case because if excess amount of HI is added into the solution, a quicker transformation of films was observed which accordingly results an irregular morphology with bigger crystallite sizes. Additionally, these uniform registries of well-defined geometry are thermodynamically stable even at ambient condition up to 6 months.

To understand the formation of different microstructures at different pH medium, we analyzed the details of the chemical components present in the reaction medium and their role at the interface. In case of heterogeneous nucleation, the particle growth via epitaxial way is very much dependent on the interaction of chemical bonds between the substrate and the deposited materials. Thus a strong deposit-substrate interaction and small lattice mismatch aid the homogeneous growth of the particle over the substrate. Additionally, the shapes of the nuclei and their subsequent growth, in turn depend on a number of thermodynamic and kinetic parameters. Depending on the chemical potential of the crystallographic faces, crystals can acquire a variety of shapes. On the other hand, reaction temperature and concentration of the solute are also another modulating parameter in determining shapes of the particle. According to the Gibbs-Wulff theorem, the development of such faces occurs in such a way that the entire crystal has a minimum total surface free energy for a given volume, i.e, $\sum_{i=1}^{n} \gamma_i a_i = \min$.

Where, a_i is the area of the i th face of a crystal bounded by n faces and γ_i is the surface free energy per unit area of the i th face. Therefore, the crystal minimizes its surface energy by enclosing its lowest possible surface energy facets. Now for fcc crystal structure, the surface

energy follows the general sequence $\gamma_{\{111\}} < \gamma_{\{100\}} < \gamma_{\{110\}}$ and coordination number (CN) follows the reverse order, i.e. CN{111}> CN{100}> CN{110}. Hence, the minimum surface energy requirement adopts tetrahedron or octahedron shape evolution enclosed by {111} facets. In general, polyhedra are more stable as truncation of the facets which provides minimum possible surface area for a given volume. Thus in progression of growth, these octahedrons try to reform themselves into truncated octahedron [26, 27] and reduce the total surface area as well as the free energy.

In our reaction mechanism, we speculate that it includes three stages. At first, formation of iodine monolayer occurs on Cu^+ interface; then nucleation starts and finally growth of the micro-crystal evolves. When Cu deposited PET substrate is immersed in the acidic solution of HI, the interfacial liquid-solid reaction takes place and metallic Copper (Cu^0) reduces to Cu^+. These copper ions promote the nucleation center to grow water- insoluble tiny CuI crystallites [23]. The possible reaction mechanism is as follows:

$$Cu^0 \xrightarrow{acidiccondition} Cu^+$$

$$HI + H_2O \rightarrow H_3O^+_{(aq)} + I^-_{(aq)}$$

$$Cu^+ + I^- = CuI$$

The reaction confirms that I^- ions in the system behave as a regulating agent to grow different crystal structures. However, selective adsorption of I^- ions on specific polar planes leads to specific directional growth to obtain such structures. An excess iodine concentration is also not helpful for morphology control rather it ceases the anisotropic shape evolution and the fast reaction process promotes bigger size isotropic crystals. In a highly symmetric zinc blende

structure, the shape of the CuI crystals is solely dependent on the surface energies of the crystallographic planes. At lower concentration of HI (pH~3), at first single crystalline tetrahedron and octahedron seeds are formed. This appearance of tetrahedron and octahedron like crystallites is the characteristic of this unit cell. The tetrahedron seeds are initially bounded by three {100} facets and a {111} base. In the evolution of growth process, these tetrahedron seeds minimize their surface energy by the development in shapes from tetrahedron to truncated tetrahedron. Similarly, the {111} planes of octahedron seeds grow and stabilize into truncated octahedron shape with six {100} and eight {111} faces. A typical schematic model representing the shape evolution process is illustrated in Figure S3 of ESI.

The growth mechanism is little different in the case of highly acidic condition (pH~1). The general tendency of the fcc unit cell is to stabilize in truncated tetrahedron shape. Hence, during the growth process, the higher concentration of iodine ions leads to the fast I^- adsorption on minimum energy planes {111} and {100} which stabilizes them rapidly one after another. Moreover, even after this quick stabilization, due to the presence of excess I^- {110} planes start growing and minimize their surface energy [28]. Thus the external morphology is the outcome of this orientational arrangement of small building block formed by truncated tetrahedrons. As a result these micro rods are bounded by two {100} side faces, two {110} truncated faces and two flat facets of {111} planes.

3.3. Optical properties:

Investigation of optical property of the CuI films was executed through UV-Vis absorption and photoluminescence (PL) analysis. Figure 4 shows the room temperature absorption spectra of the CuI films grown under pH1 and pH3 condition. Two distinct peaks can be observed in the

absorption spectra of both the films. The strongest peak located at 3.02 eV is associated with the $Z_{1,2}$ type exciton, which is basically the lowermost excitonic excitation of electrons at Γ point close to the valence band. Since the optical transitions of CuI is direct and allowed at the Γ point, $Z_{1,2}$ exciton always consists of degenerate heavy hole (HH) and light hole (LH) excitons. But, in practical systems, apart from lattice mismatch and thermally induced strain, the quantum size effect may lift this degeneracy, resulting the splitting in excitonic peak of the absorption spectra. Since the magnitude of this strain induced splitting is very small (10-15 meV) [29, 30], in our case the relaxation of degeneracy cannot be detected in the absorption spectra. Relatively less intense peak in the absorption spectra located at 3.65 eV clearly demonstrates the occurrence of spin-orbit splitting of the valence band. This peak is related to the Z_3 type exciton, which arises due to the transition of electron from spin-orbit split off band to the excitation ground state. The experimentally obtained spin-orbit splitting energy Δ_0 = E (Z_3) - E ($Z_{1,2}$) = 630 meV is in complete agreement with the values already available in the literature [31]. The full width at half maximum of the $Z_{1,2}$ excitonic absorption band was found to be 0.04 eV. Such a small value of the peak width evidently claims the highly crystalline nature of the as grown CuI films.

3.3.1. Photoluminescence analysis:

Influences of the native defects on the overall radiative and nonradiative processes in CuI has been studied by using steady state and time resolved photoluminescence (TRPL) spectroscopy which are depicted in figure 5. The room temperature steady state PL spectra of CuI films, grown under different pH environment are shown in figure 5(a) and (b). Both the films apparently consist of a primary PL emission at 410 nm. But, a closer observation towards the PL band also reveals that the pH3 CuI film evidently consists of two peaks; a sharp peak at 410 nm and a

broad peak at 421 nm. Since the position of the lower wavelength sharp emission peak exactly coincides with the low energy absorption peak, this PL band can be directly attributed due to the radiative recombination of free excitons [29]. The relatively broader and weaker emission peak located at 421 nm originates due to the recombination of electrons in conduction band with the holes trapped in the deep level surface trapping sites [32]. Moreover, it is often observed that high density of these trapping sites effectively quench the excitonic luminescence phenomenon. Therefore, a superior crystal quality is required for obtaining the defect free excitonic emission. At the same time, from the PL spectra of pH1 films, (shown in figure 5(b)) it is evident that the spectra is dominated by free excitonic emission only and the trace of the deep level emission is almost negligible. To further analyze the line width of the excitonic emission, multiple peak fitting was performed with the help of Gaussian amplitude line shape function. The rate of errors associated in this fitting process is ~0.45%, which strongly claims the reliability of the obtained parameters. Nonexistence of the defect band along with very small FWHM of the excitonic peak (~ 0.09 eV) clearly indicates the high crystal quality of the CuI films grown under pH1 condition. Since the appearance of the defect band is directly related to the native point defects present in the crystal, a careful inspection of final stoichiometry obtained from the EDX results can precisely probe the origination of the defect PL band. The films grown under pH3 condition are more susceptible to possess iodine vacancy due to availability of less I^- in the growth medium. But, due to higher concentration of I^- in the nutrient solution the films grown under pH1 condition contains very less amount of iodine vacancy. As a result, stoichiometrically rich pH1 films do not show any defect state emission whereas considerable amount of iodine vacancy present in the pH3 films are responsible for the formation of surface trapping sites. Stoichiometrically rich pH1 films do not show any defect emission whereas considerable amount

of iodine vacancy present in the pH3 films are responsible for the formation of surface trapping sites. Identification of exact reason of origination of this deep level trap has been carried out thoroughly with the help of first principles calculations which will be discussed in the subsequent section later. Further verification of the PL peak positions was confirmed with the help of cathodoluminescence (CL) analysis of the corresponding CuI films. The CL spectra (shown in the Figure S4 of ESI) clearly demonstrate that the peaks are located exactly at the same position as the PL spectra.

Detail investigation of the different dynamical processes related to the carrier recombination mechanism has been conducted with the help of TRPL spectroscopy. Moreover, TRPL also provides important information about the exciton lifetime, which is an important parameter associated with the radiative recombination efficiency and the overall optical quality of the material. The PL decay profile of the free excitonic emission as well as the deep trap emission of the CuI films grown under pH3 and pH1 condition is shown in figure 5(c) and 5(d), respectively. All the decay curves were well fitted into a bi-exponential function described by the following equation-

$$I(t) = A_1 \exp\left(-\frac{t}{\tau_1}\right) + A_2 \exp\left(-\frac{t}{\tau_2}\right) \quad (1)$$

Where τ_1 and τ_2 are the decay components of the luminescence, and A_1 and A_2 are the weighting parameters. The nature of such double-exponential decay behaviour strongly suggests that two different decay processes are involved in the emission mechanism. The fast decay component is normally attributed to the nonradiative recombination, while the slow decay component is ascribed to the radiative lifetime of the free excitonic recombination [33]. Figure 5(c) and (d) clearly indicates that the decay profile of 410 nm emission corresponding to free excitonic

recombination is slow as compared to the 425 nm emission in both the films. The average lifetime for a bi-exponential decay can be described by the equation [34]-

$$\tau_{av} = \frac{A_1\tau_1^{\ 2} + A_2\tau_2^{\ 2}}{A_1\tau_1 + A_2\tau_2} \quad (2)$$

The average life time was found to be 0.83 ns and 0.22 ns for free excitonic emission and deep level emission of the pH3 CuI films, respectively. It is interesting to perceive that, though free excitonic emission exhibits comparatively slow decay with time constants of τ_1=25.8 ps and τ_2=871 ps, still, the major decay process is unfortunately dominated by the fast decay component (61%). Generally, the PL decay time (τ_{PL}) is determined not only by radiative life time (τ_R) but also by the nonradiative decay (τ_{NR}) according to the equation [35]- $\frac{1}{\tau_{PL}} = \frac{1}{\tau_R} + \frac{1}{\tau_{NR}}$. Hence, the PL lifetime is highly interconnected with the light matter interaction such as the radiative decay of the exciton, various non-radiative processes like leak by deep-level traps, low-lying surface states and multiphonon scattering. Since τ_{NR} includes various nonradiative processes, consequently, the PL lifetime in a semiconductor relies significantly on the purity and exact synthesis condition of the sample. Presence of any kind of defect species gives rise to a quick relaxation of the excited carriers through these non radiative recombination centres and a faster decay time is obtained. In case of pH3 CuI films, considerable amount of iodine vacancy acts as non radiative recombination centres and are just sufficient to cause nonradiative decay of major part of the excitons. But the scenario is somewhat different in case of pH 1 CuI films. Being almost stoichiometric, these films contain remarkably small amount of defects, whose signature is prominent from the room temperature PL spectra. The defect free nature of the films is also manifested in terms of PL decay time of free excitonic emission which

is shown in the figure 5(d). The average life time of free excitonic emission was not only found to be increased to a value 0.91 ns with time constants τ_1=28.3 ps and τ_2=925 ps, but also the major decay process (55%) is interestingly dominated by the slower decay component (τ_2). Also the average life time of the deep level emission reduced to 0.15 ns. Above results clearly specify that dominant nonradiative recombination processes are governed by I vacancy and the density of such kind of defects play an important role in the decay of exciton population. Moreover, a clear correlation between the lifetime of free excitonic emission and the strength of the defect emission is found, which can be controlled by the precise growth the crystals.

3.4. DFT calculation and electronic structure analysis:

Going beyond the typical experimental measures, we performed first principle calculations based on density functional theory (DFT) to analytically estimate the origin of defect bands in pH 3 CuI films. Figure 6 collectively describes the close correlation of the DFT calculated results with their experimental counterpart. Enlarged view of the optimized CuI lattice with and without V_I is shown in the figure 6(a). Corresponding complete supercell structures are supplied as Figure S5 of ESI for reference. Calculated total density of states (TDOS) of both of these pure and V_I incorporated CuI structures are shown in figure 6(b). As expected, the TDOS pattern of pure CuI clearly demonstrates two distinct set of bands that are completely separated by forbidden gap. Since it is well known that the GGA-DFT calculations underestimate the band gap of any semiconductor material, so-called the scissor approximation was applied to shift the conduction band minima (CBM) to match the experimental value of separation from VBM (valance band maxima) of 3.1 eV [23, 36]. Electronic transition from these band edges gives rise to the radiative recombination of the free excitons leading to the free excitonic emission which we have

already observed in the room temperature PL spectra of the films. But, as V_I is introduced, it can be clearly seen that the TDOS pattern around the Fermi level distinctly changes and a small band near VBM appears. Recombination of electrons with the holes trapped in the deep level defect sites generates this defect band, which may almost screen the free excitonic emission if the density of such defects is sufficiently high. Notably, this DFT calculated defect band is found to arise just about 0.2 eV above the VBM, which is in excellent agreement with already available reports in the literature [37, 38]. However, the observed differences in the position of the defect band obtained from DFT and PL can be attributed due to the common GGA error for which the fundamental absorption edge may be underestimated [39]. Nevertheless, a considerable similarity can be observed in the DOS pattern and PL spectra. Additionally, a closer inspection of the TDOS indicates that the complete TDOS pattern of V_I incorporated CuI structure shifts ~0.3 eV to the lower energy side in comparison to that of the pure CuI structure. In order to experimentally confirm occurrence this phenomenon, we have examined the valence band structure of the grown CuI films with the help of X-Ray photoelectron spectroscopy as shown in figure 6(c). The valence band spectra (VBS) of pH 3 CuI films are also found to shift to the lower binding energy region by an amount ~0.3 eV with respect to the pH 1 films. This excellent corroboration highlights the acute synergy of these theoretical models to our experimentally measured data. The theoretically calculated and experimentally observed shift of valence band edge to the lower energy side can be attributed to Coulombic interactions between the electrons in the conduction band and the holes trapped in the defect sites as well as to the exchange energy of the holes [40]. Thus our theoretical calculation conclusively confirms that the existence of I vacancy in the lattice gives rise to deep level traps which we have experimentally witnessed from the room temperature PL spectra. In order to figure out the exact orbital contributions that

dominates appearance of this defect band, a precise probing of the TDOS curves were carried out by analysing the partial density of states (PDOS) of different orbitals which are shown in figure 6(d)-(f). PDOS patterns of pure and V_I introduced CuI system, both confirms the well-known notion that majority of the upper valence bands (around − 2 to 0 eV) are dominated by Cu 3d with a noticeable contribution from I 5p whereas the lower edge of the conduction band consists of Cu 4s along with a slight involvement of I 5p. A careful deconvolution of VBS into two peaks also reflects the consistency of the PDOS structures with their hybridized nature [41, 42]. Comparison of the PDOS patterns of both the systems readily implies that the localized defect state which appeared in the TDOS pattern of V_I introduced CuI structure principally originates from s orbital contribution only. Furthermore, we have shown PDOS of one of the nearest Cu atoms of the V_I site in figure 6(f). This conclusively demonstrates that the defect states are localized strongly on the Cu 4s states (indicated by the arrow) nearest to the V_I site which arises from the breakage of Cu-I bond. Moreover, the existence of localized electronic levels near the VBM can act as traps for photogenerated holes and is in accordance with the experimentally observed defect band in the room temperature PL spectra of pH 3 films.

The above inferences are also strongly supported by atomic charge density difference (CDD) diagrams as shown in Figure 7. CDD diagrams along a (1 0 -1) atomic plane (as shown in Figure 7(a), this plane passes through V_I) for both pure (Figure 7(b)) and V_I introduced CuI structure (Figure 7(c)) are shown above, where red color indicates electron enrichment and blue color indicates electron depletion. As evident from the figure, in case of V_I introduced CuI, breakage of Cu-I bonds leads to lower electronic charge sharing of the neighboring Cu atoms, which in turn manifests heightened electron enrichment at the Cu atoms in immediate vicinity of V_I sites. A quantitative analysis of this heightened charged accumulation was also performed by Mulliken

charge analysis, which shows V_I adjacent Cu atoms losing partial charge from 0.410|e| to 0.330|e| after Iodine vacancy are introduced. This localized electron accumulation is the sole underlying cause for the observed drastic change of the V_I adjacent Cu atoms' 4s orbital DOS; and from a wider perspective, it gives birth to the defect bands in V_I introduced CuI structures.

4.CONCLUSIONS:

In this report we have successfully demonstrated a novel, simple and cost effective route to fabricate CuI thin films on transparent and flexible PET substrate that can exhibit free excitonic photoluminescence at room temperature. Significant appearance of this emission band has been observed under certain experimental conditions where strength of the acidic environment played a crucial role to control the overall purity and microstructure of the grown films. A wide comparison, extracted from the analysis of different photo physical aspects not only confirms almost defect free nature of free excitonic emission from the pH1 films but also gives a direct analogy between the stoichiometry and basic luminescence characteristics of the grown films. Any deviation from stoichiometry, specifically the presence of iodine vacancy gives rise to the defect band in the PL spectra which was prominent in pH3 films. Further justification of such direct relationship between structural disorder and basic luminescence properties was supported by the first principle calculation using Density Functional Theory. DFT results clearly depict evolution of a defect band in the iodine vacancy incorporated system at ~ 0.2 eV above the VBM. These defect states are calculated to be strongly localized on the Cu 4s orbitals nearest to the V_I site and were found to originate due to breakage of Cu-I bonds. These results not only explain the experimental findings, but also clearly indicate that inherent excitonic luminescence can be realized by the precise control over the film deposition technique. Moreover, the obtained sharp and stable free excitonic emission from the reported films could be implemented directly in

the field of near UV optoelectronic applications such as LEDs and laser diodes.

NOTE AND REFERENCES:

†Electronic Supplementary Information available: Details of instrumentations and computational methods, digital image of as deposited CuI films on PET substrate under different pH conditions, survey spectra of both the thin films obtained from XPS, schematic growth mechanism of the CuI films grown under different concentration of HI, CL spectra of the thin films at room temperature, demonstration of two 2×2×2 super cell structures of the pure CuI along with V_I incorporated CuI.

Corresponding Author

*Kalyan Kumar Chattopadhyay: email: kalyan_chattopadhyay@yahoo.com

Tel.:+91 9433389445; Fax: +91 33 2414 6007

Author Contributions

‡These authors contributed equally to this work.

ACKNOWLEDGEMENTS

The authors (SD, SS & UKG) would like to thank and acknowledge the financial support from the Council of Scientific and Industrial Research (CSIR), the Government of India, for awarding Senior Research Fellowships during the execution of the work. One of us (DS) wishes to thank the W.B. State Govt. for providing fellowships during the execution of this work. We also wish to thank the Department of Science & Technology (DST) of the Government of India, University Grants Commission for 'University with Potential for Excellence scheme (UPE-II)' and TEQIP programme for financial help.

REFERENCES:

1. C. Zhang and J. Lin, *Chemical Society reviews*, 2012, **41**, 7938-7961.
2. Y. Zhang and J. Hao, *Journal of Materials Chemistry C*, 2013, **1**, 5607-5618.
3. D. Vanmaekelbergh and L. K. van Vugt, *Nanoscale*, 2011, **3**, 2783-2800.
4. R. K. Joshi and J. J. Schneider, *Chemical Society reviews*, 2012, **41**, 5285-5312.
5. S. T. Kochuveedu, Y. H. Jang and D. H. Kim, *Chemical Society reviews*, 2013, **42**, 8467-8493.
6. M. I. Utama, J. Zhang, R. Chen, X. Xu, D. Li, H. Sun and Q. Xiong, *Nanoscale*, 2012, **4**, 1422-1435.
7. J. Singh, P. Kumar, K. S. Hui, K. N. Hui, K. Ramam, R. S. Tiwari and O. N. Srivastava, *CrystEngComm*, 2012, **14**, 5898-5904.
8. I. Chung, J. H. Song, J. Im, J. Androulakis, C. D. Malliakas, H. Li, A. J. Freeman, J. T. Kenney and M. G. Kanatzidis, *Journal of the American Chemical Society*, 2012, **134**, 8579-8587.
9. J. W. Drewitt, P. S. Salmon, S. Takeda and Y. Kawakita, *Journal of physics. Condensed matter : an Institute of Physics journal*, 2009, **21**, 075104-075113.
10. S. Hull, *Reports on Progress in Physics*, 2004, **67**, 1233-1314.
11. H. Ichida, Y. Kanematsu, T. Shimomura, K. Mizoguchi, D. Kim and M. Nakayama, *Physical Review B*, 2005, 72, 045210-045214.
12. D. Huang, Y.-J. Zhao, S. Li, C.-S. Li, J.J. Nie, X.-H. Cai and C.M. Yao, *Journal of Physics D: Applied Physics*, 2012, **45**, 145102-145108.
13. M. Knupfer, *Applied Physics A: Materials Science & Processing*, 2003, **77**, 623-626.

14. Z. Chen, F. Ding, F. Hao, Z. Bian, B. Ding, Y. Zhu, F. Chen and C. Huang, *Organic Electronics*, 2009, **10**, 939-947.

15. H. Sirringhaus, *Advanced Materials*, 2005, **17**, 2411-2425.

16. H. Iimori, S. Yamane, T. Kitamura, K. Murakoshi, A. Imanishi and Y. Nakato, *The Journal of Physical Chemistry C*, 2008, **112**, 11586-11590.

17. T. Tanaka, K. Kawabatab and M. Hirose, *Thin Solid Films*, 1996, **281-282**, 179-181

18. P. M. Sirimanne, M. Rusop, T. Shirata, T. Soga and T. Jimbo, *Materials Chemistry and Physics*, 2003, **80**, 461-465.

19. S. L. Dhere, S. S. Latthe, C. Kappenstein, S. K. Mukherjee and A. V. Rao, *Applied Surface Science*, 2010, **256**, 3967-3971.

20. B. Huang, Z. Zheng, F. Yang, Y. Zhang, D. Pu, H. Zhao and D. Li, *Solid State Ionics*, 2008, **179**, 2006-2010.

21. H.Y. Huang, D.J. Chien, G.-G. Huang and P.Y. Chen, *Electrochimica Acta*, 2012, **65**, 204-209.

22. Z. Zheng, A. Liu, S. Wang, B. Huang, K. W. Wong, X. Zhang, S. K. Hark and W. M. Lau, *Journal of Materials Chemistry*, 2008, **18**, 852-854.

23. X. Hu, J. C. Yu, J. Gong and Q. Li, *Crystal Growth & Design*, 2007, **7**, 262-267.

24. S. Ntais and A. Siokou, *Surface Science*, 2006, **600**, 4216-4220.

25. S. Ntais, V. Dracopoulos and A. Siokou, *Journal of Molecular Catalysis A: Chemical*, 2004, **220**, 199-205.

26. Z. L. Wang, *The Journal of Physical Chemistry B*, 2000, **104**, 1153-1175.

27. J. L. Elechiguerra, J. Reyes-Gasga and M. J. Yacaman, *Journal of Materials Chemistry*, 2006, **16**, 3906-3919.

28. R. Kozhummal, Y. Yang, F. Guder, U. M. Kuc-ukbayrak and M. Zacharias, *Acs nano*, 2013, **7**, 2820–2828

29. D. Kim, M. Nakayama, O. Kojima, I. Tanaka, H. Ichida, T. Nakanishi, and H. Nishimura, , *Physical Review B*, 1999, **60,** 13879-13884

30. M. Nakayama, M. Kameda, T. Kawase and D. Kim, *Physical Review B*, 2011, **83**, 235325-235329

31. A. Blacha, S. Ves and M. Cardona, *Physical Review B*, 1983, **27**, 6346-6362.

32. Y. Yang and Q. Gao, *Langmuir*, 2005, **21**, 6866-6871

33. Y. Zhong, A. B. Djurisic , Y. F. Hsu, K. S. Wong, G. Brauer, C. C. Ling and W. K. Chan, *J. Phys. Chem. C,* 2008, **112**, 16286–16295

34. S. Saha, S. Das, U. K. Ghorai, N. Mazumder, B. K. Gupta and K. K. Chattopadhyay, *Dalton transactions*, 2013, **42**, 12965-12974.

35. S. W. Jung, W. I. Park, H. D. Cheong, G.C. Yi, H. M. Jang, S. Hong and T. Joo, *Applied Physics Letters*, 2002, **80**, 1924-1926.

36. H. Wang, X. Bai, J. Wei, P. Li, Y. Jia, H. Zhu, K. Wang and D. Wu, *Materials Letters*, 2012, **79**, 106-108.

37. Y. Xu, D. Chen, X. Jiao and L. Ba, *J. Phys. Chem. C*, 2007, **111**, 6-9

38. Y. Zhou, M. lü, G. Zhou, S. Wang and S. Wang, *Materials Letters*, 2006, **60**, 2184-2186.

39. H. Peng and J. Li, *J. Phys. Chem. C*, 2008, **112**, 20241–20245

40. J. A. Silberman, T.J. de Lyon and J.M. Woodall, *Applied Physics Letters*, 1991, **58**, 2126-2128.

41. A. Goldmann, J. Tejeda, N. Shevchik and M. Cardona, *Physical Review B*, 1974, **10**, 4388-4402.

42. J.G. Gross, M. Fliyou, S. Lewonczuk and J.Ringeissen, *Physical Review B*, 1988, **37**, 3068-3074

Figure caption:

Fig. 1: XRD pattern of the CuI thin films on PET grown under pH1 and pH3 condition. The star marks indicate the position of the substrate peaks. XRD pattern of standard JCPDS data card is also shown for easy comparison with the sample data.

Fig. 2: (a-b) EDX pattern of the CuI thin films grown under pH3 and pH1 condition, respectively. (c-d) Representation of high resolution XPS spectra of Cu 2p and I 3d core level of both the films, respectively.

Fig. 3: Microstructural evolution of CuI thin films while going from pH3 (a-d) to pH1 (e-h) growth environment, respectively. (a&e) FESEM images showing the morphology of CuI thin films (b&f) TEM images of truncated octahedra and microrod like structures grown under pH3 to pH1 acidic medium, respectively. (c&g) HRTEM images showing the uniform lattice fringes as a representation of highly crystalline nature of the samples. (d&h) SAED pattern of the microstructures showing their single crystalline characteristics.

Fig. 4: Room temperature absorption spectra of CuI thin films.

Fig. 5: (a-b) Room temperature PL spectra of CuI thin films excited at 370 nm UV excitation. (c-d) Photoluminescence decay profiles of CuI thin films grown under pH3 to pH1 acidic medium, respectively. In all cases, the hollow and solid spheres represent experimental curve while the fitted curves are represented by the lines.

Fig. 6: (a) Enlarged view of the optimized CuI structure with and without iodine vacancy. (b) Calculated total density of states (TDOS) for the pure and V_I incorporated CuI structures. (c) High resolution valence band spectra of the corresponding CuI structures where black line denotes the experimental curve while the fitted curves are represented by the blue lines. (d &e)

Partial density of states plot for pure and V_I incorporated CuI structures, respectively. (f) PDOS pattern for the nearest Cu of V_I site.

Fig. 7**:** Atomic charge density difference (CDD) diagrams for pure and V_I incorporated CuI structures along a (1 0 -1) plane indicated by the green area.

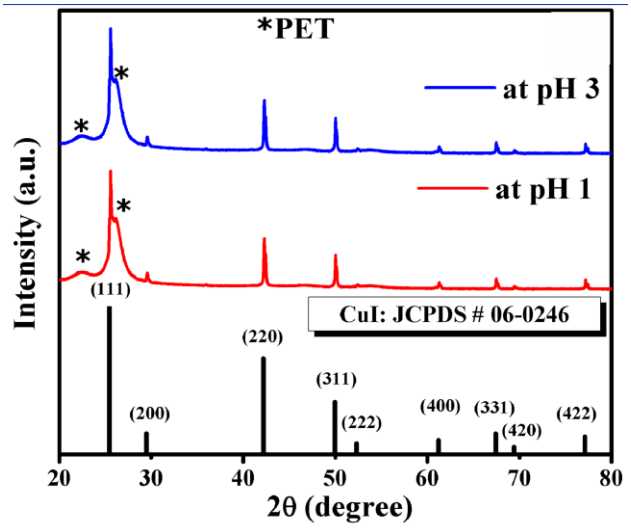

Fig. 1

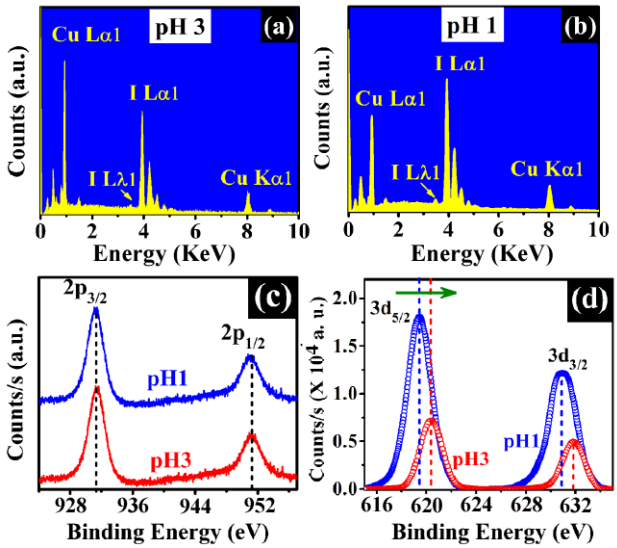

Fig. 2

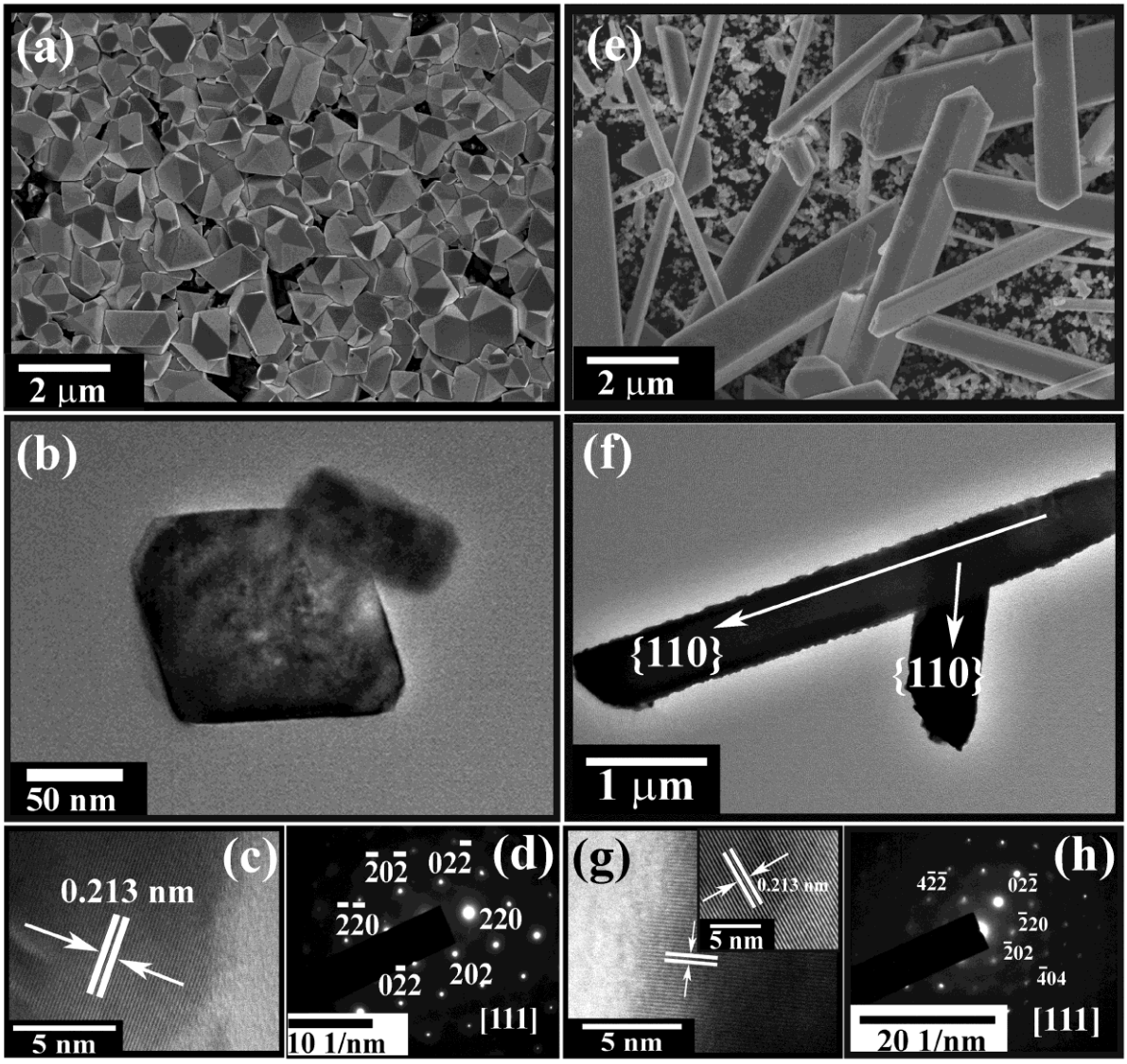

Fig. 3

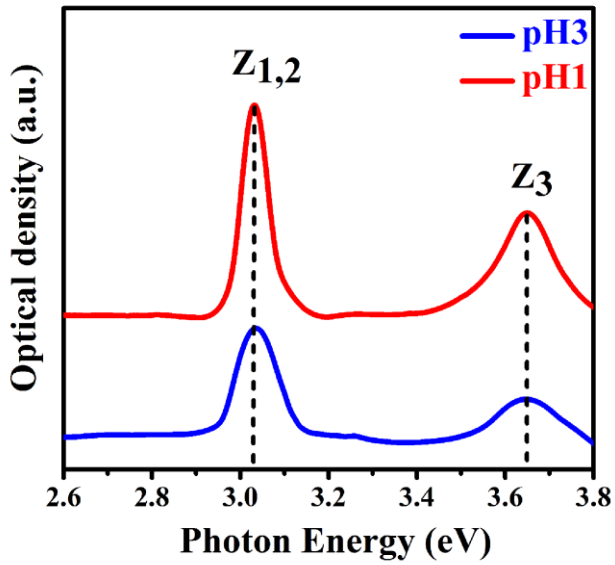

Fig. 4

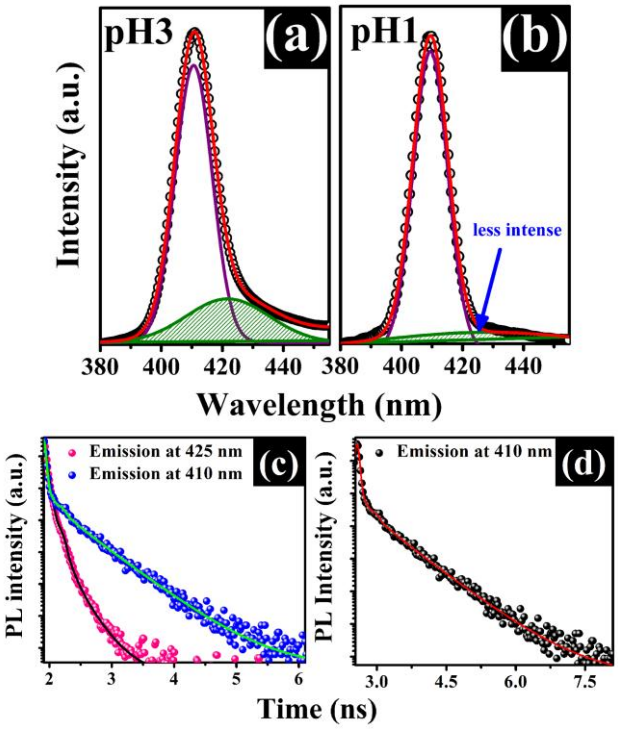

Fig. 5

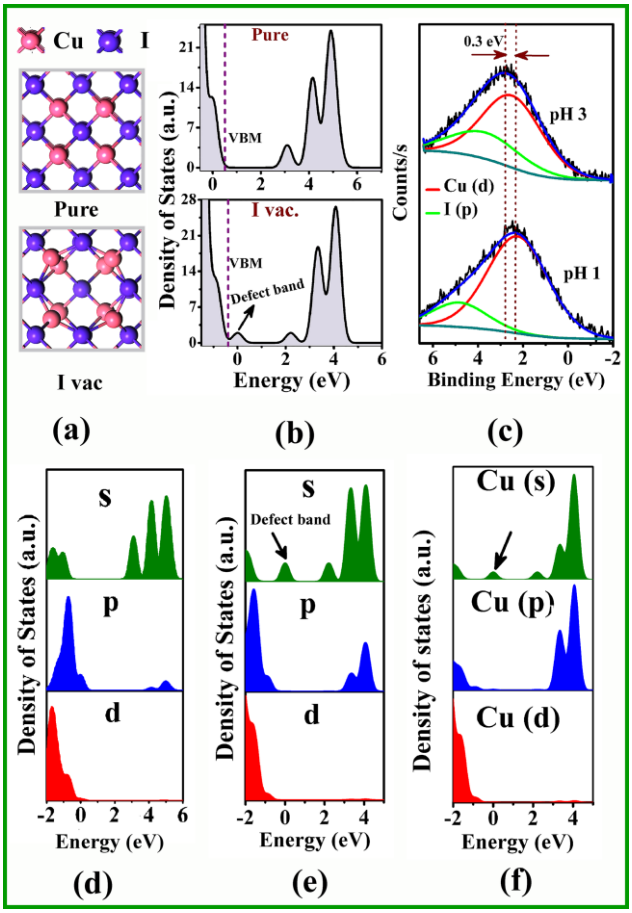

Fig. 6

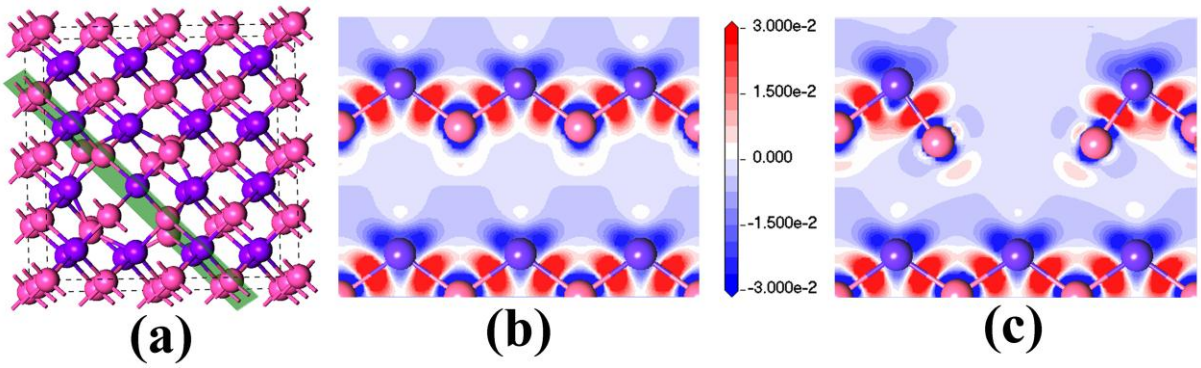

Fig. 7

TABLE OF CONTENT:

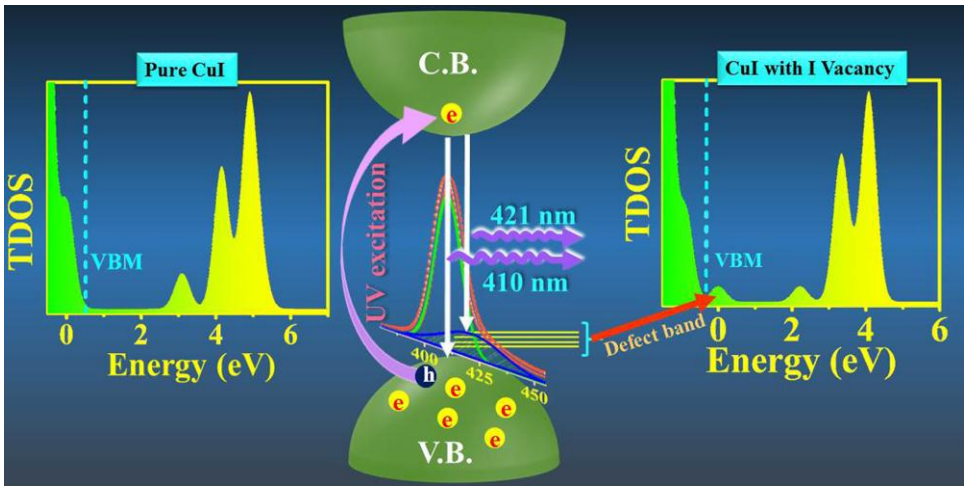

Iodine concentration modulated free excitonic emission of CuI thin films developed by wet chemical reaction at room temperature.